Final Technical Report

Submitted to the U.S. Geological Survey

USGS Award Number: G12AP20020

Title of Award: 3D structural velocity model of the Santa Maria basin, California, for improved strong ground motion prediction

Authors: John H. Shaw and Andreas Plesch, Department of Earth & Planetary Sciences, Harvard University, Cambridge, MA 02138
shaw@eps.harvard.edu // 617 495-8008
andreas_plesch@harvard.edu // 617 495-2356

Contract Term: January 1 to December 31st, 2012

Abstract
We developed a new 3D structural velocity model of the Santa Maria basin in southern California to serve as a basis for improved estimates of hazardous ground shaking that will result from future earthquakes in the region. The new model includes a detailed description of the basin shape, represented by top-basement and other geologic horizons. These surfaces are constrained by dozens of petroleum wells, seismic reflection profiles, and maps and geologic cross sections. To ensure that these surfaces are compatible with the positions and offsets of major faults, we constructed three-dimensional representations of the Orcutt, Lompoc, Casmalia, Los Alamos, San Marcos, and Zaca faults within the basin. Locations of these faults, along with others from the SCEC Community Fault Model (CFM) (Plesch et al., 2007), were used to constrain the basement surface, including areas where basement is offset and repeated by thrusting. This basement surface and topography were used to define a basin volume, within which the velocity structure of the sediments was constrained by a database of dozens of sonic logs. These well data show a general trend of increasing velocity (Vp) with depth to maximum values of about 4500 m/s. However, velocities vary significantly across the basin due to structures and lithologic changes, and there are several local velocity inversions (area where velocities decrease with depth). To represent this complex velocity structure, the model was parameterized for Vp using geostatistical interpolation methods (kriging) that have been successfully applied to model velocity structure in other sedimentary basins in California, including the Los Angeles basin (Süss and Shaw, 2003). Shear wave (Vs) and density models were subsequently developed using the general empirical relationships of Brocher (2005).

The new Santa Maria basin model has been embedded in the SCEC Community Velocity Model (CVM-H), replacing the basin description that was included in version 11.9. The new model is comprised of a series of voxets (Vp, Vs, and density) that can be accessed through the SCEC UCVM framework. This framework offers a flexible code that allows users to populate their own computation meshes with our model's Vp, Vs, and density parameterizations. In addition, the model consists of topography, top basement, and fault surfaces that are also available through an ftp site. The faults surfaces will be incorporated as new and alternative representations in a subsequent release of the SCEC Community Fault Model (CFM).

Delivery of the model through the SCEC UCVM framework will enable its evaluation and use in a wide range of applications. This will include numerical simulations of seismic wave propagation by investigators employing various numerical techniques, including finite difference, finite element, and spectral element methods (e.g., Aagaard et al., 2001; Antolik et al., 1996; Bielak et al., 1999; Boore, 1972; Chen et al., 2007; Frankel and Vidale, 1992; Komatitisch et al., 2004; McLaughlin and Day, 1994; Minster et al., 2004; Olsen, 2000; Tromp et al., 2005). Through comparisons of observed and synthetic waveforms, these studies will help to further calibrate the models and provide strong ground motion predictions for future large earthquakes in southern California in the form of synthetic waveforms and peak ground displacement, velocity, and acceleration maps.

Tectonics and structure of the Santa Maria basin
The Santa Maria basin (Figure 1) is located in the Western Transverse Ranges of southern California (Reed and Hollister, 1936; Vedder et al., 1969), and marks the western limit of this active, east-west trending zone of deformation (Yeats, 1983; Namson and Davis, 1988a; Shaw

and Suppe, 1994). Geologic studies of folding and faulting (e.g., Namson and Davis, 1988a; Yeats et al., 1988; Yeats 1983, 1988; Yeats and Huftile, 1995; Huftile and Yeats, 1995; Shaw and Suppe, 1994; Kamerling et al., 2001; Pinter, 2003) and present-day stress measurements (Mount and Suppe, 1992) in the Transverse Ranges indicate that both regional contraction and compression are directed north-south to northeast-southwest, sub-normal to the San Andreas fault (Zoback et al., 1987; Hauksson, 1990). Shortening across the fold-and-thrust belt resolves a component of the discrepancy between the relative Pacific-North American plate motion and observed slip on the San Andreas fault (Minster and Jordan, 1978).

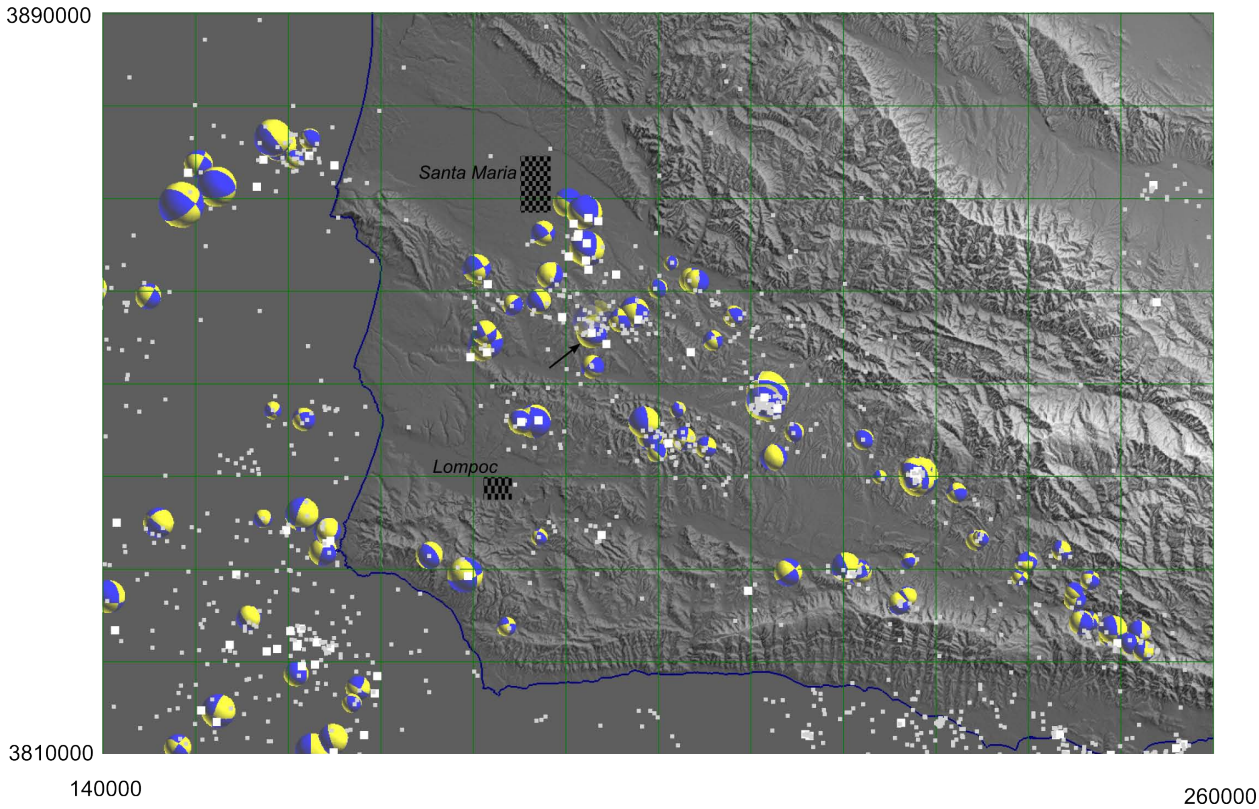

Figure 1: Map of the Santa Maria basin showing seismicity (white dots, from Hauksson et al. 2011) and focal mechanisms solutions (Hauksson et al. 2010; upper hemisphere projection) used in this study to constrain basin structure. Larger dots indicate M > 3. The arrow points to the M3.5 1991 event associated with the Orcutt oil field operations (Kanamori and Hauksson, 1992). Coordinates at corners are in the UTM zone 11 projection, NAD 1927. Coordinates in all subsequent maps are in the same system.

The Santa Maria Basin is roughly 100 km long and up to 50 km wide at its maximum extents. The basin shallows to the southwest as it terminates into the northwest trending Santa Lucia Range and San Rafael Mountains (Namson and Davis, 1990). The eastern side of the basin is divided by the San Rafael Mountains, separating the basin into two shallow and narrow lobes. To the west, the basin continues offshore into the Pacific Ocean, where it is bounded by the Hosgri fault system. The basin is filled with Tertiary and Quaternary sediments lying unconformably above Mesozoic metasedimentary and igneous rocks. The lowermost Tertiary stratigraphic unit in the basin is the Monterey Fm., a deepwater marine shale of early Miocene age. The Sisquoc Fm., a Miocene to Pliocene marine clastic section, lies above the Monterey shale. In turn, this

section is overlain by Quaternary sediments over most of the study area. In the center of the basin, this Quaternary section is up to 1 km thick.

The Santa Maria basin began to develop about 20 million years (Ma) ago, during a regional episode of extensional tectonism (Kieniewicz, 1986; Chen and Oertel, 1988; Namson and Davis, 1990). The central basin was formed, in part, due to displacement on a series of high-angle normal faults. Between 3 and 5 Ma ago, the regional tectonics transitioned to the modern transpressional regime (Chen and Oertel, 1988; Namson and Davis, 1990; Gutierriez-Alonso and Gross, 1997), creating thrust faults and reactivating some of the normal faults as high-angle reverse faults. This deformation created the dominant structural features of the present-day basin, which include three major anticlines separated by two synclines, all trending roughly N120°E. Many of the major faults within and bounding the basin have been active in the Quaternary. On November 4, 1927 a M7.1 Earthquake ruptured offshore of Lompoc, possibly on the Hosgri Fault System. The Santa Ynez fault last ruptured in the Quaternary, and the Big Pine Fault, on the eastern boundary of the basin, may have ruptured in the Holocene (WGCEP, 2007). The Little Pine and Los Alamos faults, both within the basin, also ruptured in the late Quaternary and Holocene, respectively (WGCEP, 2007). Namson and Davis (1990) show further evidence for active blind thrust faults underlying the folds in the basin. Recent models forecast rupture events of M5.5 or greater on these blind thrust faults every 80-300 years, and every 50-300 years on the southern Hosgri fault system (Ward, 2007).

The structure of the Santa Maria basin is very important in the context of strong ground motions studies and seismic hazard. The basin is deep, with total sediment thicknesses locally exceeding 3000 m. Moreover, the basin is elongated in an east-west direction, with locally steep northern and southern borders that are formed largely by displacements on blind-thrust and reverse faults, as well as associated folds. Several structures extend into the sedimentary basin, locally thrusting higher velocity basement rocks over lower velocity sediments. Similar velocity inversions in the Santa Monica region of the Los Angeles basin were shown to have focused and amplified seismic waves during the 1994 Northridge (M 6.7) earthquake (e.g., Graves et al., 1998; Davis et al., 2000). Thus, characterizing the structure of the basin is critical to properly assessing the distributions of hazardous ground shaking that will result from large earthquakes on faults surrounding the basin, as well as other significant earthquakes on more distant sources such as the San Andreas fault.

The surface geology and subsurface structure of the Santa Maria basin has been studied by various authors (e.g., Dibblee, 1950; Hill and Dibblee, 1953; Kieniewicz and Luyendyk, 1986; Chen and Oertel, 1989; Namson and Davis, 1990; Gutierrez-Alonso and Gross, 1997; Onderdonck et al., 2005), and a rich history of oil and gas exploration has spurred the acquisition of high-resolution seismic reflection and well data in the region. We have used results of these studies along with additional data constraints to construct a three-dimensional structural model of the basins that includes structural characterization of the basin shape and fault systems, as well as velocity and density parameterizations for the basin sediments. Our approach to constructing and testing this model is described in the following sections.

Constructing the models

Basin structure

In order to properly describe the size and shape of the basin in the new model, we first need to incorporate topographic/bathymetric and geologic surfaces that are used to specify property boundaries. As in the CVM-H (Süss and Shaw, 2003; Plesch et al., 2009), the new Santa Maria model contains topography and bathymetry derived from GTOPO30, a global digital elevation model provided by the U.S. Geological Survey, and offshore depth soundings made available through the Army Corps of Engineers. For geologic horizons, the base of the Tertiary section, corresponding locally to the top of Mesozoic sedimentary, metasedimentary, and igneous rocks, was chosen to describe the bottom of the basin. Sonic logs show that this "acoustic" basement horizon represent an abrupt change in velocity and density.

The basement and other geologic surfaces were constructed by integrating published maps, wells, seismic reflection profiles, and cross sections (Figure 2). These data and interpretations were precisely georeferenced, and integrated in Gocad (Mallet, 1992), a 3-D geologic CAD tool specializing in the construction of surfaces, the analysis of spatially distributed data, and the modeling or simulation of properties. The base-Tertiary surface has been mapped in outcrop with great precision around the basin (Dibblee Map Series, 1950-2005), and is easily recognizable in wells and logs in many parts of the Santa Maria basin. Moreover, several authors have used balanced cross sections and potential field data to define this surface across the basin (Kieniewicz and Luyendyk, 1986; Chen and Oertel, 1989; Namson and Davis, 1990).

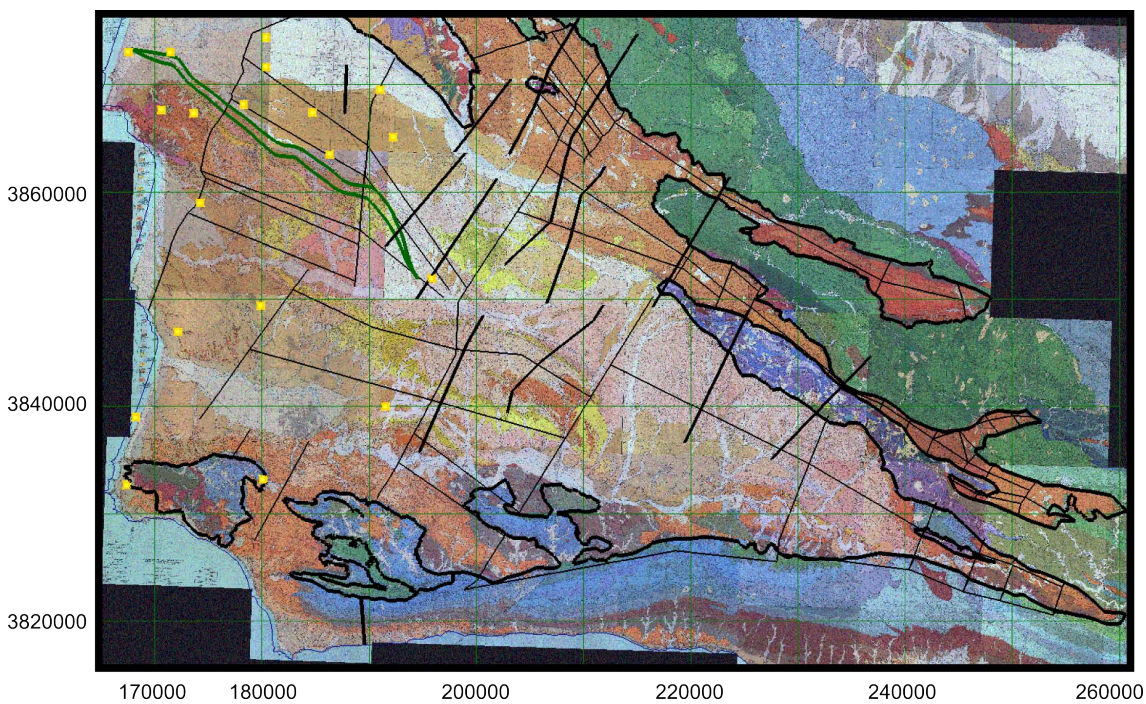

Figure 2: Map of data used to constrain the geometry of the top basement surface, including Dibblee maps (Dibblee 1950-2002) and geologic sections (straight black lines) from Dibblee (1950-2002), Namson and Davis (1990), and other sources. The bold black contact in the map represents the base Tertiary at outcrop. Green polygon: Orcutt fault offset of base Tertiary. Yellow squares are wells that penetrate the basement surface.

An important aspect of properly constraining the basin structure was to ensure that geologic horizons are compatible with the locations and displacements of major faults. For large faults bounding the basin, we used fault representations from the SCEC Community Fault Model (CFM 4) (Plesch et al., 2007). However, the CFM did not include representations of many of the faults within the basin. Thus, we expanded our efforts to include the development of new representations for several of the major faults in the area, including the Orcutt, Lompoc, Casmalia, Los Alamos, San Marcos, and Zaca faults. To constrain these new fault models, we used the USGS Quaternary Fault & Fold database to define surface traces, and a range of subsurface data including seismicity, well logs, structure contour maps from oil fields, and cross sections (Figure 3). For the seismological data (Figure 1), we incorporated a series of new, relocated earthquake catalogs that offer much improved hypocentral locations and a larger focal mechanism database that was used to constrain subsurface fault geometries (Shearer et al., 2005; Lin et al., 2007; Hauksson et al., 2011).

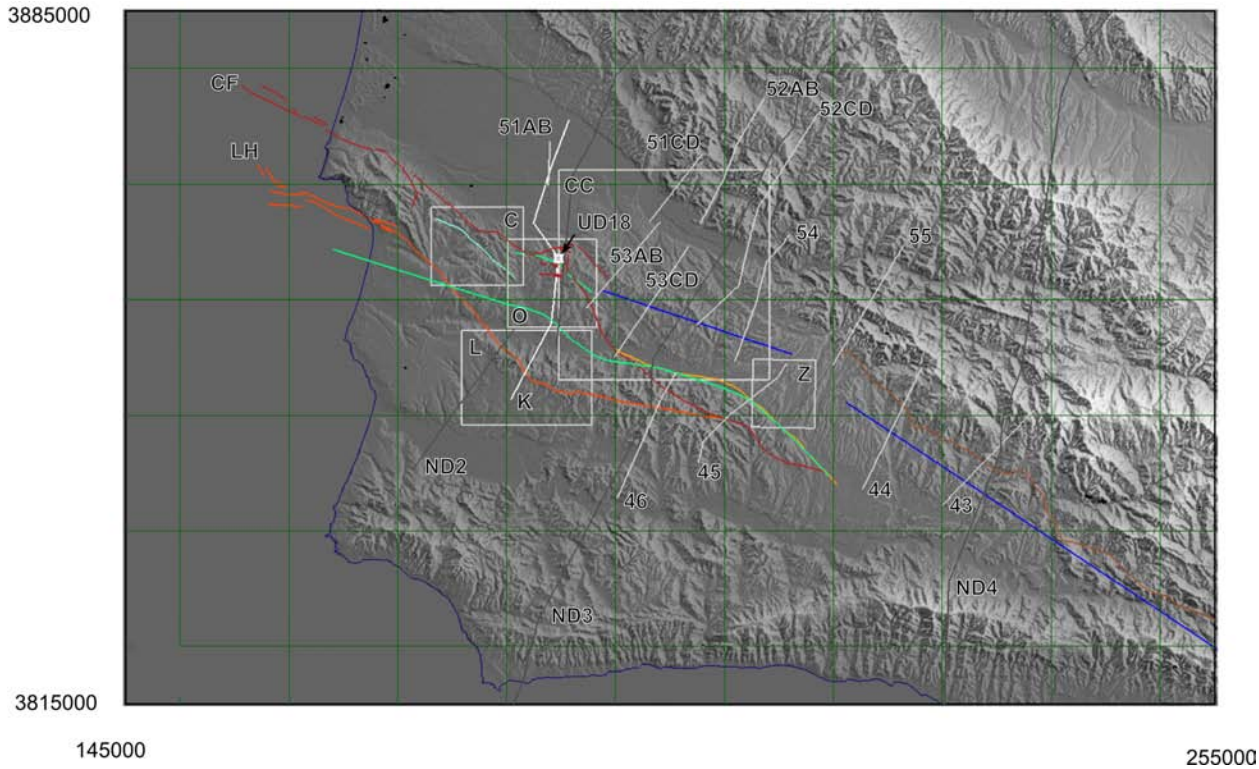

Figure 3: Map showing data used to construct faults representations. Red, light red, and orange lines are USGS Quaternary Fault & Fold Database traces (CF: Casmalia fault; LH: Lions Head fault; orange: Los Alamos fault). Green trace is fold axis based on Dibblee (1950-2002). Grey boxes are areas of oil field structure contour maps with well coverage (C: Casmalia field; O: Orcutt field; L: Lompoc field; CC: Cat Canyon field; Z: Zaca field). Grey and white lines are cross-sections from Dibblee (1950-2002), Namson and Davis (1990), and Krammes et al. (1952). Numbers reflect Dibblee (1950-2002) section designations. ND2-4 are Namson and Davis (19XX) cross-sections. K: Krammes et al. (1952) correlation section. Arrow points to well Union Dome-18 (UD18).

Brief descriptions of these fault characterizations are provided below:

Orcutt fault: This fault was not included in the SCEC CFM, but has been recognized in the Orcutt oil field, and represented in previously published cross-sections (Krammes et. al., 1959; DOGGR, 1992). The fault extends along strike across the Orcutt and Casmalia oil fields (Figure 4), and there is no direct constraint on its eastern termination. Lettis et al. (1995) describe the Orcutt fault as another name for the Casmalia fault citing others. However, our analysis of detailed maps from the oil fields and the surface trace of the Casmalia fault suggest that they are distinct structures. Specifically, a well cut of the Orcutt suggests that it is a blind reverse fault dipping to the south, with the Casmalia fault (described below) located in its hanging wall. The sense and magnitude of displacement on the Orcutt fault suggests that it distinctly offsets the basement horizon, and thus has been used to constrain the geometry of this surface in our model.

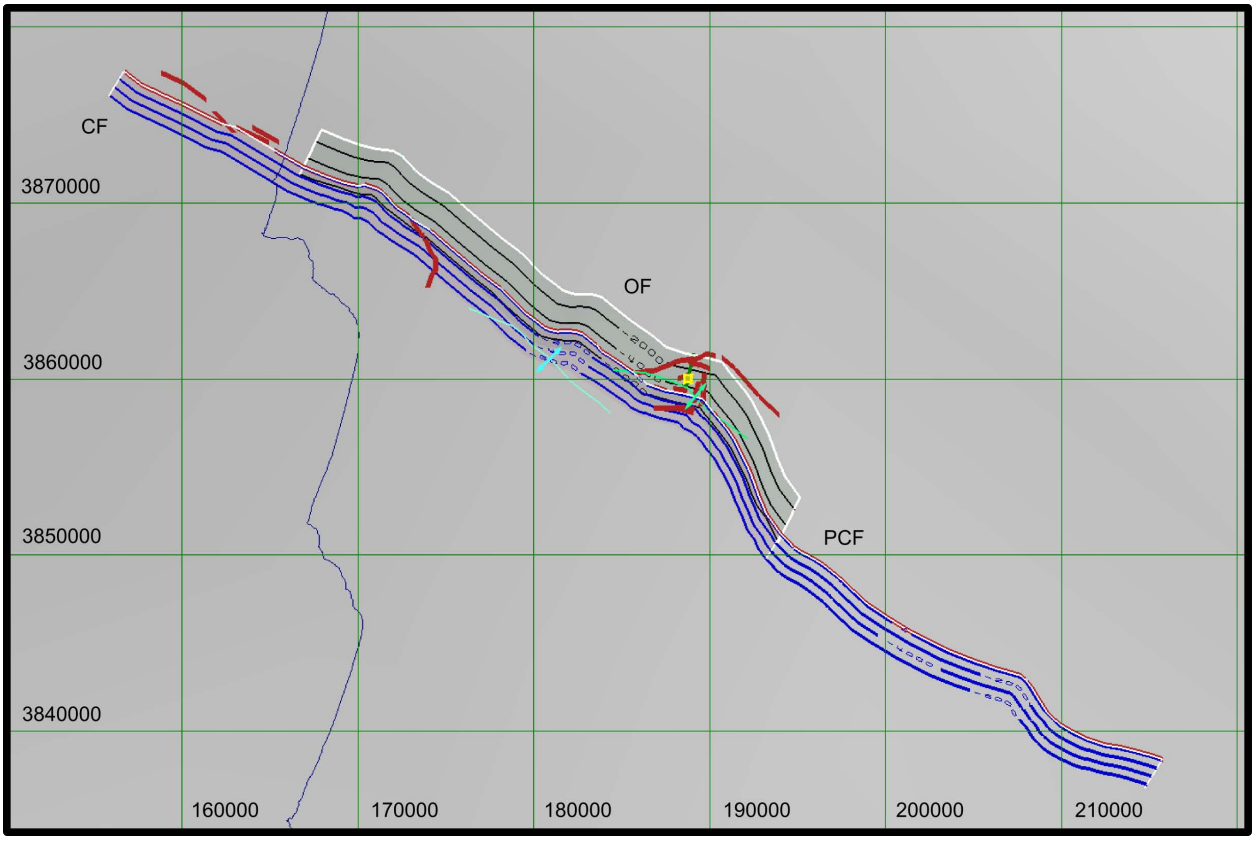

Figure 4: Contour maps (2000 m contour interval) of the blind Orcutt reverse fault (OF, black contours), the Casmalia fault (CF, blue) and the Pezzoni-Casmalia fault section (PCF, blue). Red: USGS qfault trace of Casmalia fault; blue and green are anticlinal axes from oil field maps. The yellow symbol is the Union Dome-18 well, which drilled through the Orcutt fault.

Casmalia fault: This fault was included in the CFM based on the surface trace of Jennings (1994). However, we refined the fault representation using more precise traces from the USGS Quaternary Fault & Fold Database and subsurface maps from the Orcutt field. Based on the surface traces, we divided the fault into two sections, the Casmalia fault in the west and the Pezzoni-Casmalia fault in the east (Figure 4). The Casmalia fault dips steeply to the southwest,

and is generally considered to have component of right-lateral strike-slip displacement (Hardebeck, 2010). The Casmalia fault lies in the hangingwall of the Orcutt fault, but based on our interpreted fault dips the two structure do not intersect at depth above the base of our model (Figure 5). Nevertheless, they may interact at depth and partition oblique convergence into strike- and dip-slip components. Due to its predominantly strike-slip displacement, the Casmalia fault does not have a major impact on the geometry of the basement surface.

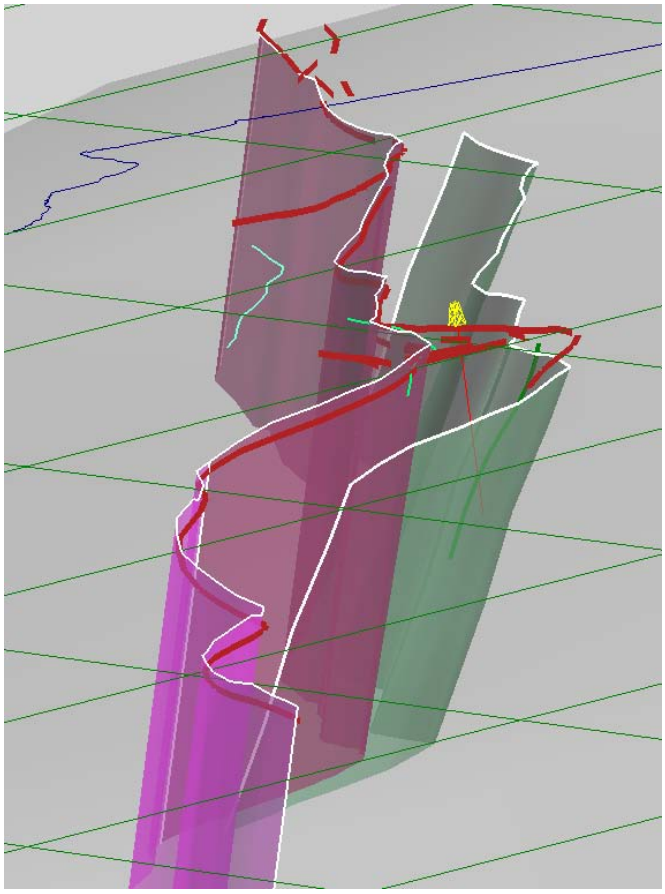

Figure 6: Perspective view of the Casmalia fault (purple) and the blind Orcutt reverse fault (green), looking to the west. Red lines are USGS qfault traces. The Union Dome-18 well is shown, which drilled through the Orcutt fault.

Los Alamos and Lompoc faults: These faults were not included in the SCEC CFM, but were interpreted in our study using traces from the USGS Quaternary Fault & Fold Database, surface and subsurface geology, and seismicity (Figure 6). The faults lie in the southeastern part of the basin. The trace of the Los Alamos faults runs generally parallel to the Los Alamos syncline (Dibblee, 1950-2005). The syncline has a steeply dipping southern limb that defines the northern edge of the Lompoc anticlinorium. Namson and Davis (1990) interpreted the Lompoc anticlinorium as a fault-bend fold formed by displacement on an underlying blind-thrust ramp termed the Purisima-Solomon fault. Based on the highly asymmetric, north-vergence of the Lompoc anticline and Los Alamos syncline, we suggest as an alternative interpretation that this structure represent a tip-line or fault-propagation fold (Suppe and Medwedeff, 1990; Erslev, 1991; Allmendinger, 1998; Shaw et al., 2005). Based on this assessment, we revise our interpretation of the Purisima-Solomon fault (here termed the Lompoc thrust) such that it dips

moderately to the southwest and extends upwards to the base of the Los Alamos syncline (Figure 7). The depth of the thrust ramp is constrained by seismicity, which includes several focal mechanisms that have nodal planes parallel to the inferred thrust ramp. The Los Alamos fault is interpreted as a high-angle breakthrough of the Lompoc fault along the synclinal axis of the fold (Figure 7). Near surface dips of this fault defined by the Dibblee maps (Dibblee, 1950-2005) and the USGS Quaternary Fault & Fold Database trace are used to model this fault surface. The interpreted Lompoc fault does not directly offset the basement surface, but explains the origin of the Lompoc anticlinorium, which is a prominent feature represented in the basement surface. The displacement at depth on the Los Alamos fault appears to be modest, but is not defined directly by the data and therefore is not be represented as an offset in the basement surface.

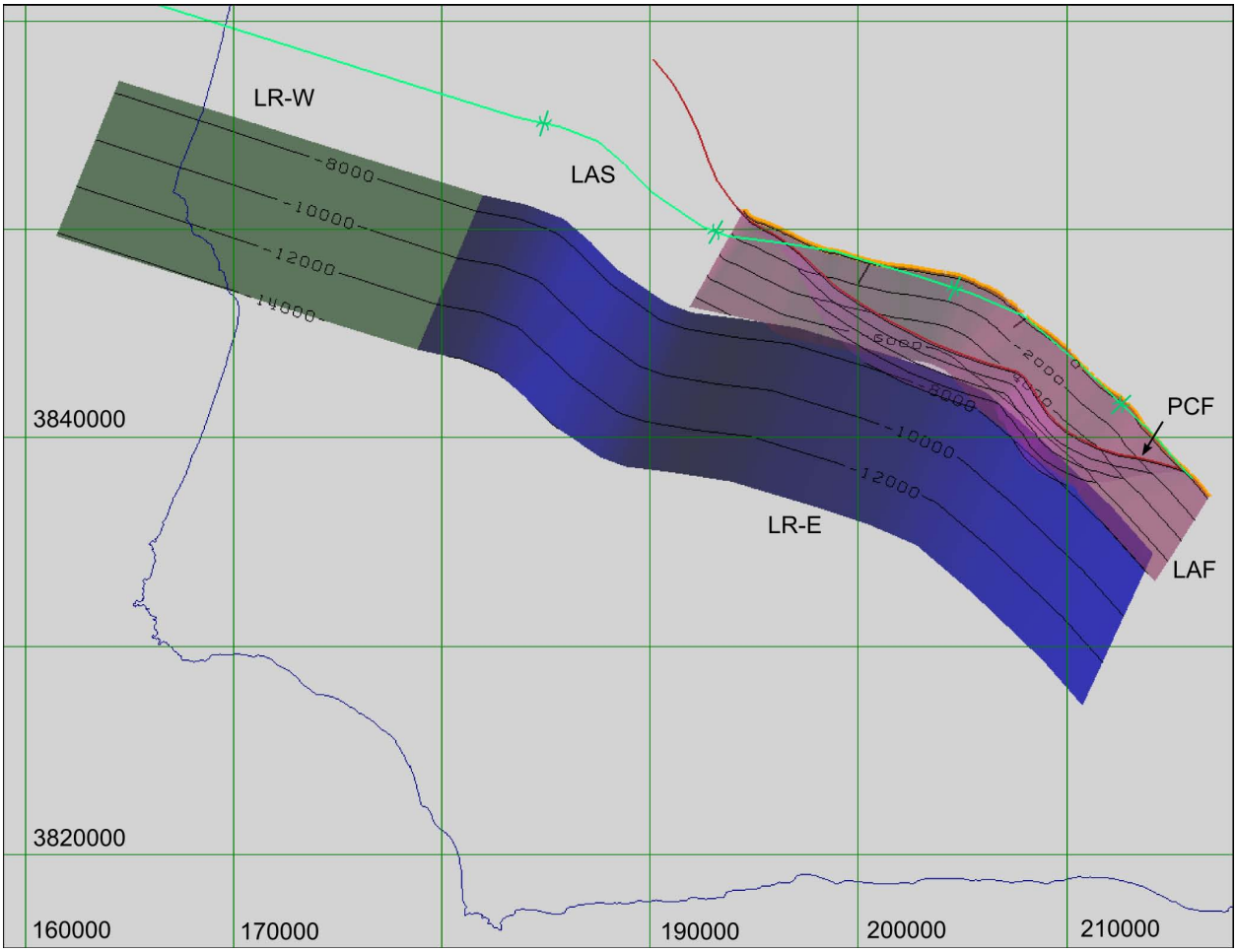

Figure 6: Contour maps (contour interval 2000 m) of the western (LR-W, green) and eastern Lompoc thrust ramp (LR-E, blue), the Los Alamos fault (LAF, purple), and the Pezzoni-Casmalia fault (PCF). The green trace is the axis of the Los Alamos syncline (LAS).

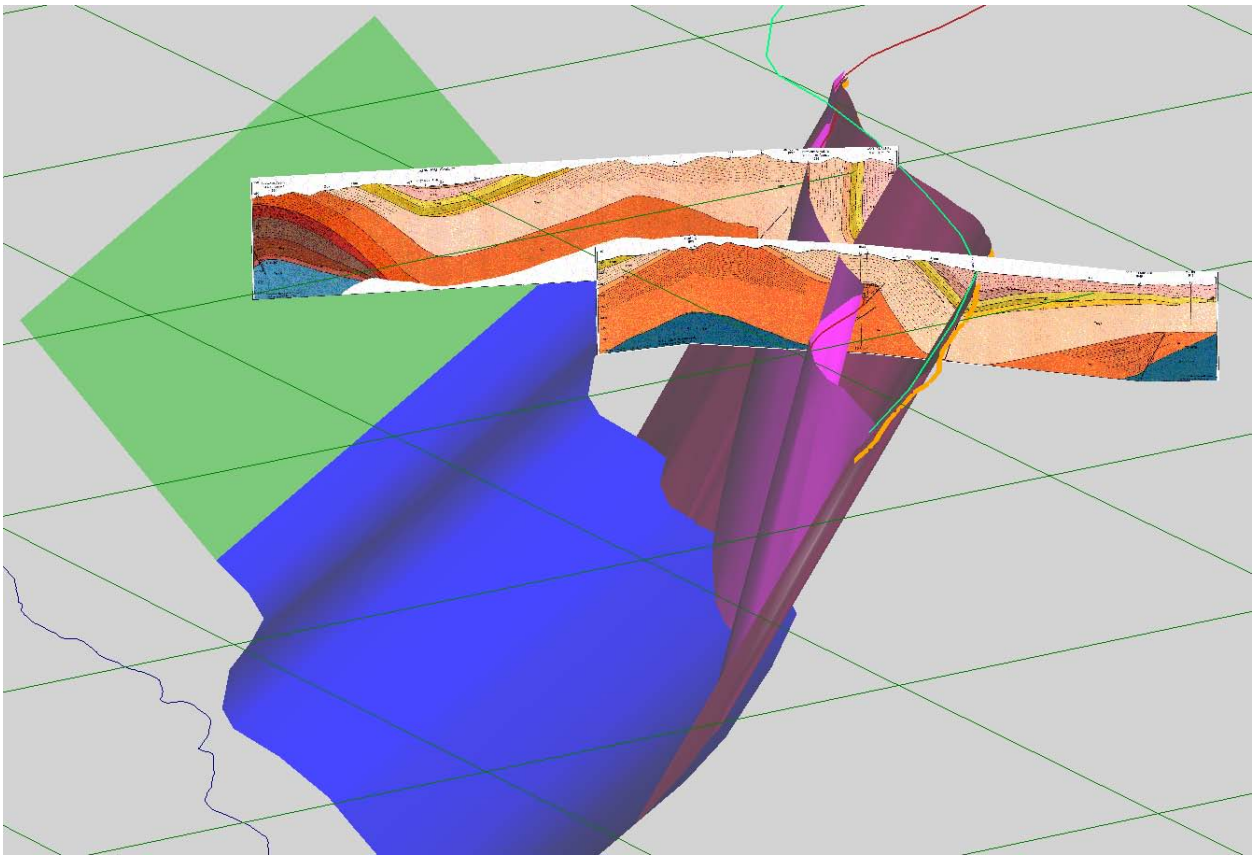

Figure 7: Perspective view of the Lompoc ramp (blue and green), the Los Alamos fault (dark red) and the Pezzoni-Casmalia fault (purple). The two cross sections are from Dibblee (1950-2002) showing the geometry of the Los Alamos syncline and the Lompoc anticline.

Zaca and San Marcos faults: These two blind faults are not represented in the CFM or the USGS Quaternary Fault & Fold Database, but rather are inferred solely based on hypocentral locations and focal mechanism solutions. The Zaca fault is defined based on hypocentral locations from Kanamori & Hauksson (1992) and cluster of seismicity to the east in the Hauksson et al. (2011) and Lin et al (2007) relocated earthquake catalogs (Figure 8). Northwest-southeast trending nodal planes from several focal mechanisms along trend were used to define the moderate southwest dip of the Zaca fault. The San Marcos fault is interpreted based on a trend of seismicity in the footwall of the north-dipping Little Pine fault (Figure 9). The dip of the San Marcos fault is not well constrained by the seismicity, but appears to be steeply north dipping.

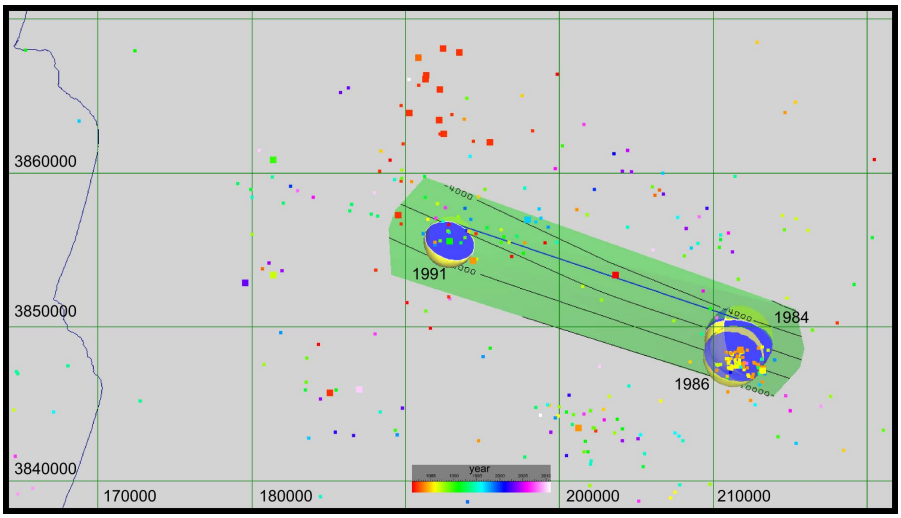

Figure 8: Contour map (2000 m contour interval) of the Zaca fault. The strike of the fault plane of the 1991 focal mechanism projects into a cluster of earthquakes just north of the Zaca oil field. The largest events of this cluster have focal mechanisms similar to the 1991 event.

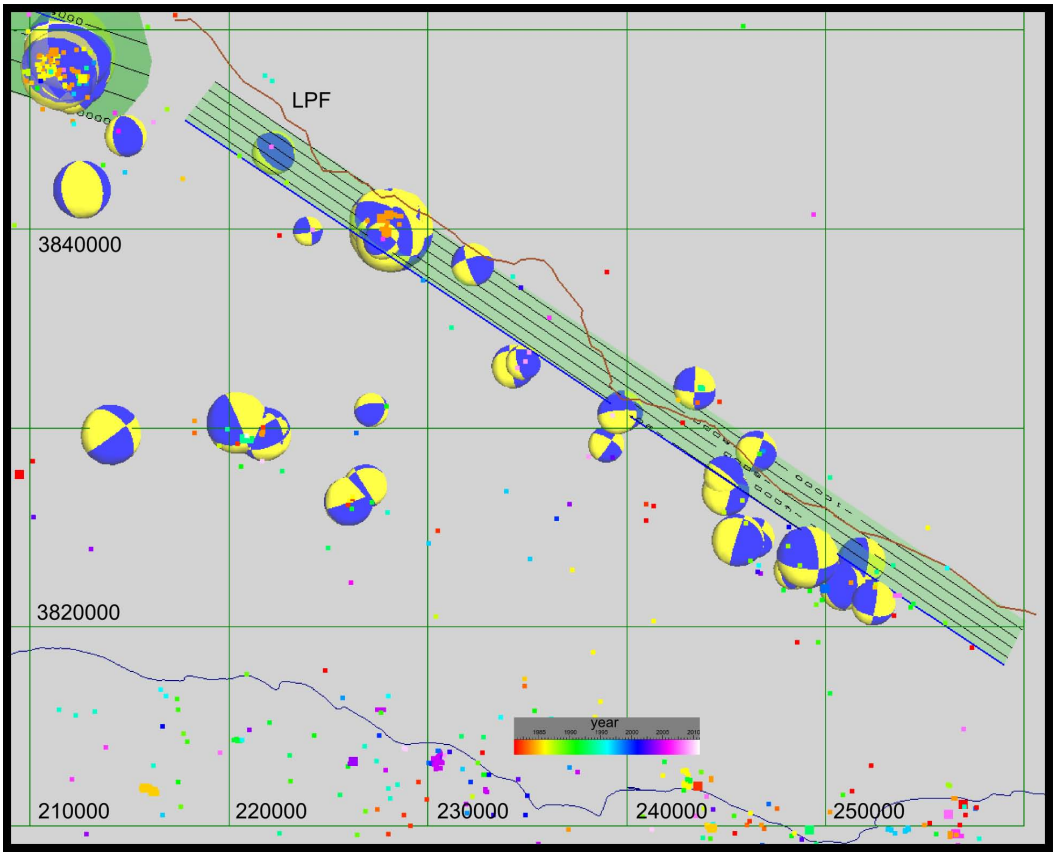

Figure 9: Contour map (2000 m interval; from 2000 m to 10000 m depth) of the San Marcos fault in the footwall of the Little Pine fault (brown trace).

Interpolating the basement surface

We developed a basement surface using the direct well picks, the surface outcrop trace, and constraints from the geologic cross sections (Figure 2), along with these new fault representations. The surface was interpolated from these direct constraints using Discrete Smooth Interpolation (DSI) as implemented in Gocad (Mallet, 1992). The basement surface was then directly offset by the Orcutt fault, using constraints on the fault displacement from the subsurface cross sections. The result is a 3D representation of the basin shape that is compatible with the locations and displacements of major fold trends and fault surfaces (Figure 10).

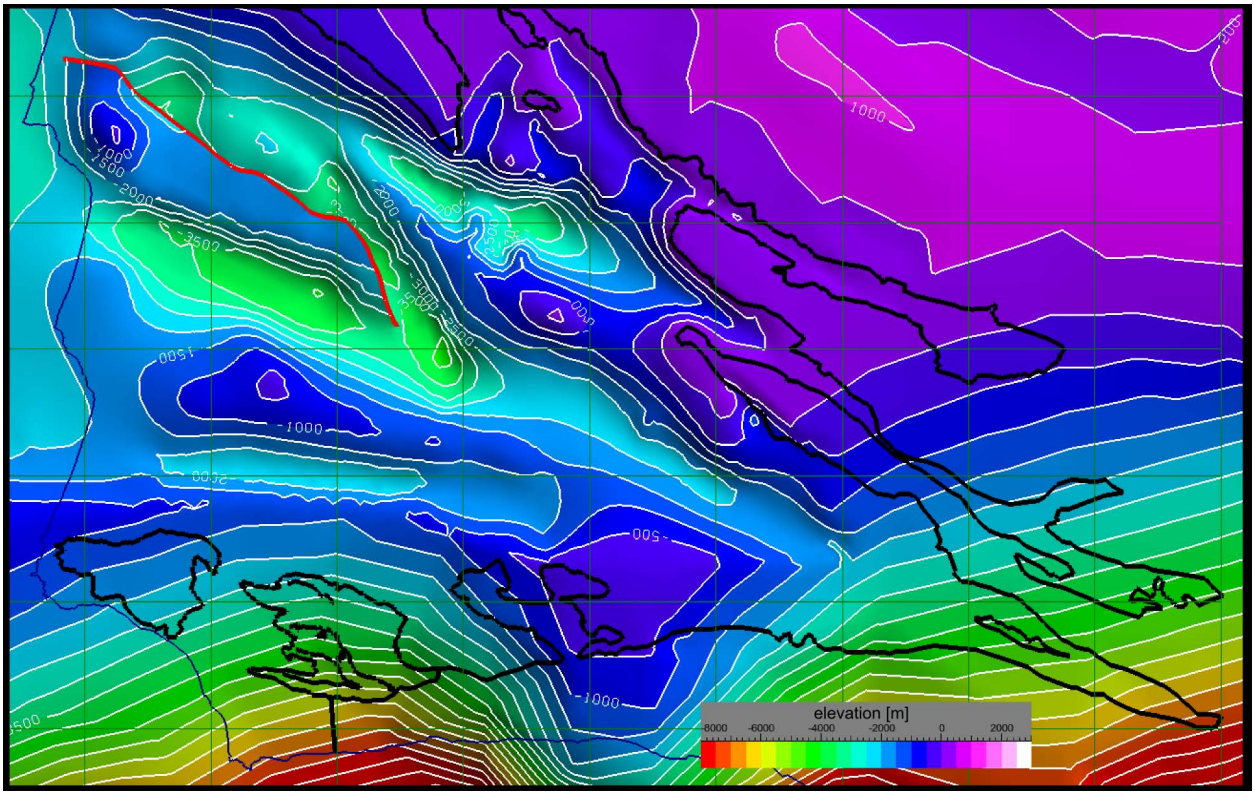

Figure 10: Contour map (500 m interval) of the basement surface. The bold black line is the outcrop of the surface. The red line is the hangingwall cut-off at the blind Orcutt reverse fault.

Model parameterization

Within the enveloping topographic and top basement surfaces, we developed a topologically regular grid in order to interpolate the velocity structure. We described the seismic velocities in the basin using a database of more than 55 sonic logs and stacking velocity measurements from industry reflection profiles. These formerly proprietary data offer extremely precise and accurate measures of P wave velocities. The different observational methods sample velocities at different scales, between audible and ultrasonic (10 versus 104 Hz) frequencies, and were smoothed to a 25 m sample for their integration into the velocity model using the approach of Süss and Shaw (2003). This yielded tens of thousands of interpolated and 25-ms-averaged velocity measurements (Figure 11).

The new three-dimensional velocity model has a horizontal grid size of 250 by 250 m and a depth grid size of 100 m, similar to the representations of other basins embedded in the SCEC CVM-H. To guide the interpolation of this model, we employed spatial relationships between the measured velocities determined through geostatistical analysis. These interpolation methods are similar to conditional stochastic techniques and are based on established geostatistical relationships [Wackernagel, 1998]. The employed functions are available in Gocad and are widely used to model natural anisotropy of physical data in geology and related disciplines. A major advantage of the kriging method is the prevention of clustering effects that can occur when dealing with unevenly distributed data. The major disadvantage of method is that it has a tendency to underestimate the full range of property values. If dealing with spatially very sparse data sets and with only local correlation, many of the estimations will equal the mean of the data.

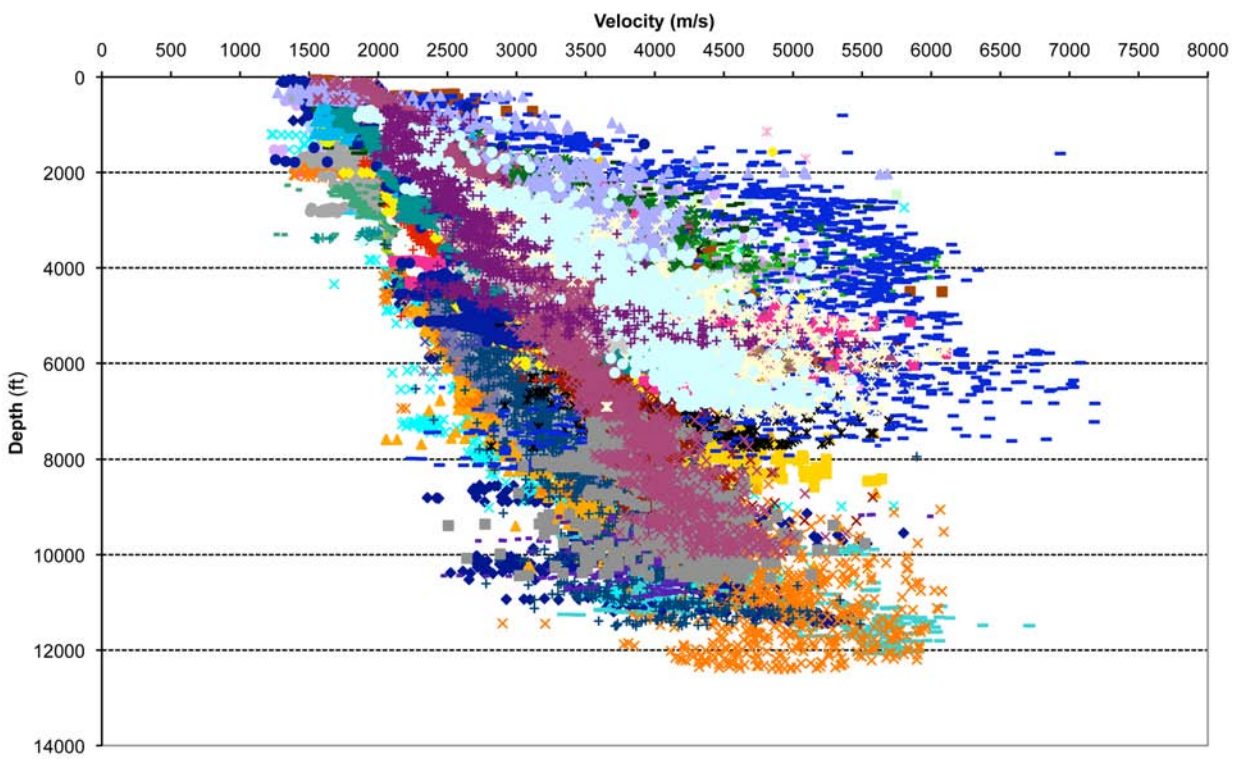

Figure 11: Plot of velocity (Vp) versus depth from sonic logs in the petroleum wells used in this study. Colors represent values from different wells. In general, Tertiary sediments show a gradually increasing velocity with depth. Wells that record higher velocities (> ≈ 4000 m/s) at shallow depths (< 8000 ft) generally penetrate pre-Tertiary acoustic basement.

In preparation for the interpolation, we parameterized the kriging function using variogram analysis following the approach of Munster (2007). The variogram analysis plots the correlation of data points based on separation distance. The distance at which data points cease to be correlated defines the limits to which data values should be associated in the interpolation. The zero-correlation distance often varies depending upon the orientation of analysis. Correlation along the strike of a structure, for example, will be greater than the correlation in an orientation perpendicular to the strike. We found that the sonic log data remains correlated for 20km along a trend of N120E, an orientation roughly parallel to the trend of the basin structure. Correlation ceased after 10km along an orthogonal orientation. These parameters define the orientation and

axes of the correlational ellipse that was used in the kriging interpolation.

Based on the interpolated Vp model, we then generated co-registered shear wave (Vs) and density models using the general empirical relationships of Brocher (2005) using the approach of Plesch et al. (2009).

Model description

The completed basin model was then embedded into the SCEC Community Velocity Model (CVM-H) 11.9 (Figure 12). The CVM-H included a definition of crustal velocity and density structure based on travel time tomography (after Hauksson, 2000) that was iteratively improved using adjoint tomographic techniques (Tape et al., 2009; 2010). The velocity structure at shallow depths is characterized by velocities around 1900 m/s, with slow velocities reflecting thick Quaternary sediments. Small velocity (~150 m/s) inversions occur in the basin between 400 m and 1000 m depth, particularly in regions characterized by intrusive igneous rocks at or near the surface. At depth and along the basin edges the velocity structure that is characterized by a strong contrast between basin sediments and basement. Basin velocities range from 1900 to 4500 m/s, generally increase with depth. In contrast, basement velocities just beneath the basin range from 5000 to 5500 m/s. Velocities variability also increases with depth, yielding velocity inversions within the deepest parts of the basin (~3300 m depth to 3800 m depth) of up to ~500 m/s.

The kriging process based on the correlation ellipsoid is responsible for the horizontal orientation of lenticular velocity structures within the basin model. In general, these velocity structures are similar to the shape and orientations of the major anticlines and synclines in the basin. Given that beds dips rarely exceed 30 º, we suggest that these predominantly horizontal velocity structures are a reasonable representation of basin structure. An alternative parameterization would likely require a detailed mapping of stratigraphic horizons within the basin, as well as an understanding of how velocities varied in each of these units. One area in the basin where bed dips are very steep is the southern limb of the Los Alamos syncline. In this area our model is expected to underestimate velocities as the older and faster strata within this limb were not sampled sufficiently by well logs.

Finally, the introduction of an offset in the basement surface of up to 1700 m is reflected in the model by a wedge of lower velocities placed under high velocities in the core of the Orcutt-Casmalia anticlines. Although the discretization of the model limits the representation of this wedge structure somewhat, it is recognized as a first order feature and is expected to have important implications for ground motion prediction through wave propagation studies. Similar wedge structures were shown to have a focusing effect on ground motions, for example in the Los Angeles basin (Graves et al., 1998; Davis et al., 2000).

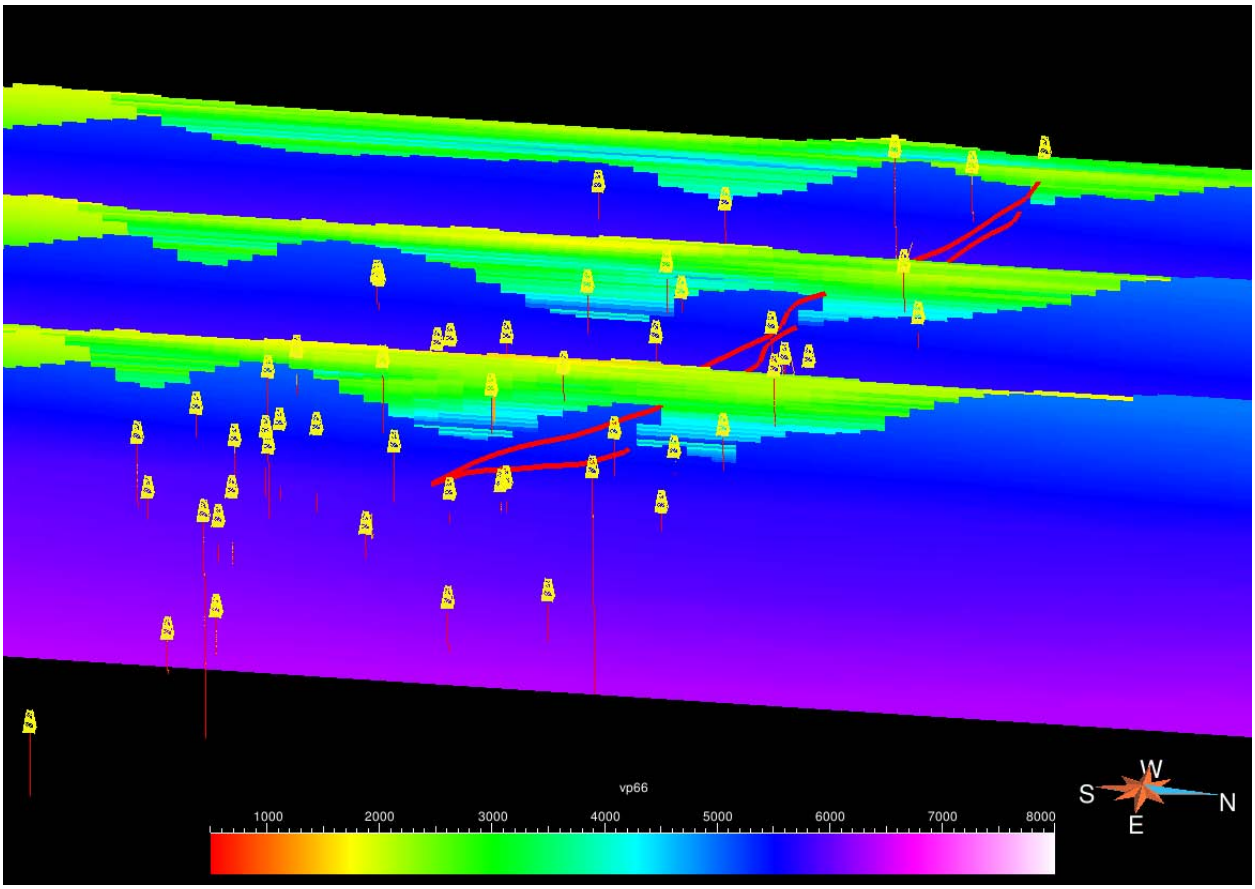

Figure 12: Three N-S cross-sections through velocity model showing the Vp velocity structure in m/s. The red lines footwall and hangingwall cut-offs at Orcutt fault. Yellow well heads with red paths are wells with sonic log data used in the model parameterization.

Summary of Results

In summary, this effort has yielded co-registered Vp, Vs, and density models for the Santa Maria basin, incorporating topography and bathymetry, as well as geologic horizons that define the basin shapes. The horizons are consistent with the locations and displacements on major fault systems represented in the SCEC CFM (Plesch et al., 2006), as well as new fault representations that we have developed. The new basin model has been embedded in the regional SCEC Community Velocity model (CVM-H), and all model components will be made available through the SCEC UCVM Framework, which is part of the Community Modeling Environment (CME) website. Delivery of the new Santa Maria model through the SCEC UCVM helps ensure that users can populate their own computation meshes using our model's Vp, Vs, and density parameterizations. This flexible distribution approach helps facilitate the use of the model for a variety of different purposes by investigators employing different computational meshes and methods. Our expectation is that the new Santa Maria models will be used by various groups to perform finite-difference, finite element, and spectral element wave propagation simulations. These studies will help both to evaluate the models, through comparisons of observed and synthetic waveforms, and improve the accuracy of strong ground motion predictions that will result from future earthquakes in the region.

References

Aagaard, B. T., J. F. Hall, and T. H. Heaton (2001). Characterization of near-source ground motions with earthquake simulations, *Earthquake Spectra 17,* no. 2, 177–207.

Allmendinger, R. (1998). Inverse and forward numerical modeling of trishear fault propagation folds: *Tectonics*, v. 17, no. 4, p. 640-656.

Antolik, M., S. Larsen, D. Dreger, and B. Romanowicz (1996). Modeling broadband waveforms in central California using finite differences, *Seismological Research Letters 67*, 30.

Bielak, J., J. Xu, and O. Ghattas (1999). Earthquake ground motion and structural response in alluvial valleys, *Journal of Geotechnical Geoenvironmental Engineering 125*, 413–423.

Boore, D. M. (1972). Finite difference methods for seismic wave propagation in heterogeneous materials, in *Methods in Computational Physics*, Vol. 11, Academic, New York.

Brocher, T.M., 2005, A regional view of urban sedimentary basins in Northern California based on oil industry compressional-wave velocity and density logs, Bulletin of the Seismological Society of America, vol.95, no.6, pp.2093-2114.

Chen, R. T. and Oertel, G. (1989). "Strain history of the Los Prietos syncline, Santa Maria basin, California: a case of post-tectonic compaction." Journal of Structural Geology 11(5): 539-551.

Chen, P., L. Zhao, and T. H. Jordan (2007), Full 3D tomography for the crustal structure of the Los Angeles region, Bull. Seis. Soc. Am., 97 (4), 1094–1120.

Davis, P. M., J. L. Rubenstein, K. H. Liu, S. S. Gao, and L. Knopoff, (2000). Northridge earthquake damage caused by geologic focusing of seismic waves, Science, 289, 1746–1750.

Dibblee, T. W., Jr. (1950). "Geology of southwestern Santa Barbara County, California-Point Arguello, Lompoc, Point Conception, Los Olivos, and Gaviota quadrangles." 95 pp.

Dibblee, T. W., Jr. 1950-2005. Geologic map series, California [Map]. 1:24,000. Santa Barbara, CA:Thomas W. Dibblee, Jr. Geol. Found.

DOGGR (California Department of Conservation, Division of Oil, Gas and Geothermal Resources) (1992), California Oil & Gas Fields Volume II – Southern, Central Coastal, and Offshore California Oil and Gas Fields, Publication No. TR12, 3rd edition.

Erslev, E. (1991). Trishear fault-propagation folding: *Geology*, v. 19, p. 617-620.

Frankel, A., and J. Vidale (1992). A three-dimensional simulation of seismic waves in the Santa Clara valley, California, from the Loma Prieta aftershock, *Bulletin of the Seismological Society of America 82*, 2045–2074.

Graves, R.W., Pitarka, A., Somerville, P. G., 1998, Ground-motion amplification in the Santa Monica area; effects of shallow basin-edge structure, Bulletin of the Seismological Society of America, vol.88, no.5, pp.1224-1242.

GutierrezAlonso, G. and Gross, M. R. (1997). "Geometry of inverted faults and related folds in the Monterey Formation: implications for the structural evolution of the southern Santa Maria basin, California." Journal of Structural Geology 19(10): 1303-1321.

Hauksson, E. (2000). Crustal structure and seismicity distribution adjacent to the Pacific and North America plate boundary in southern California, *J. Geophys. Res.* 105, 13,875–13,903.

Hauksson, E. (1990). Earthquakes, faulting and stress in the Los Angeles Basin: Journal of Geophysical Research, v. 95, p. 15365-15394.

Hauksson, E., W. Yang, and P. Shearer (2011). Waveform Relocated Earthquake Catalog for Southern California (1981 to 2011), SCEC Annual Meeting, Palm Springs, CA.

Hardebeck, J. L., (2010), Seismotectonics and Fault Structure of the California Central Coast, BSSA Bull., v. 100 no. 3, p. 1031-1050.

Hill, M. L. and Dibblee, T. W. (1953). "San Andreas, Garlock, And Big Pine Faults, California - A Study Of The Character, History, And Tectonic Significance Of Their Displacements." Geological Society of America Bulletin 64(4): 443.

Huftile, G. J. and R. S. Yeats, 1995, Convergence rates across a displacement transfer zone in the western Transverse ranges, Ventura basin, California, *J. Geophys. Res.* 100, 2043-2067.

Isaacs, C. M., and Tomson, J. H., (1990). Reconnaissance study of petroleum source-rock characteristics of core samples from the Sisquoc and Monterey Formations in a north south subsurface transect across the onshore Santa Maria basin and in surface sections along the Santa Barbara-Ventura coast, Southern California: U.S. Geological Survey Open-File Report 89-108,43 p.

Jennings, C. W. (Compiler) (1994). Fault activity map of California and adjacent areas, California Department of Conservation, Division of Mines and Geology, Geologic Data Map No. 6, scale 1:750,000.

Ji, C., D. V. Helmberger, and D. J. Wald (2000). Basin structure estimation by waveform modeling: forward and inverse methods, *Bulletin of the Seismological Society of America 90*, 964–976.

Kamerling, Marc J ; Sorlien, Christopher C ;Archuleta, Ralph ;Nicholson, Craig, 2001, Three-dimensional geometry and interactions of faults and structures along the northern margin of the Santa Barbara Channel, California, AAPG Bulletin, vol.85, no.6, pp.1127-1128.

Kanamori, H., and E. Hauksson (1992), A slow earthquake in the Santa Maria basin, California, Bull. Seis. Soc. Am., 82 (5), 2087–2096.

Kieniewicz, P. M. M. and Luyendyk, B. P. (1986). "A gravity model of the basement structure in the Santa Maria Basin, California." Geophysics 51(5): 1127-1140.

Komatitsch, D., Q. Liu, J. Tromp, P. Süss, C. Stidham, and J. H. Shaw (2004), Simulations of Ground Motion in the Los Angeles Basin Based upon the Spectral Element Method, *Bulletin of the Seismological Society of America 94*, 187-206.

Krammes, K. F., and Curran, J. R., and others (1959). Correlation section across Santa Maria basin from Cretaceous outcrop in Santa Ynez Mountains northerly to Franciscan outcrop north of Santa Maria River, California: American Association of Petroleum Geologists Pacific Section Correlation Section 12.

Kristek, J., P. Moczo, K. Irikura, T. Iwata, and H. Sekiguchi (1999). The 1995 Kobe mainshock simulated by 3D finite differences, in *The Effects of Surface Geology on Seismic Motion*, K. Irikura, K. Kudo, H. Okada, and T. Sasatani (Editors), Vol. 3, Balkema, Rotterdam, The Netherlands, 1361–1368.

Larsen, S., M. Antolik, D. Dreger, C. Stidham, C. Schultz, A. Lomax, and B. Romanowicz (1997). 3-D models of seismic wave propagation: Simulating scenario earthquakes along the Hayward fault, *Seismological Research Letters 68*, 328.

Lettis, W. R., Hanson, K. L. , Unruh, J. R., McLaren, M. and W. U. Savage (2004), Quaternary Tectonic Setting of South-Central Coastal California, USGS Bull. 1995-AA.

Lin, G., P. M. Shearer, and E. Hauksson (2007). Applying a three-dimensional velocity model, waveform crosscorrelation, and cluster analysis to locate southern California seismicity from 1981 to 2005, *J. Geophys. Res.*, **v.112**, n.B12, 14 pp, B12309, doi:10.1029/2007JB004986.

Lysmer, J., and L. A. Drake (1972). A finite element method for seismology, in *Methods in Computational Physics*, Vol. 11, Academic, New York.

Magistrale, H., S. Day, R. W. Clayton, and R. Graves (2000), The SCEC Southern California Reference Three-Dimensional Seismic Velocity Model Version 2, *BSSA 90*, S65-S76.

Mallet, J. L., Discrete smooth interpolation in geometric modeling, *Comput. Aided Design*, 24(4), 178–191, 1992.

McLaughlin, K. L., and S. M. Day (1994). 3-D elastic finite-difference seismic wave simulations, *Computational Physics 8, no. 6*, 656–663.

Minster, J., Olsen, K B. Moore, R., Day, S., Maechling, P., Jordan, T., Faerman, M., Cui, Y., Ely, G., Hu, Y., Shkoller, B., Marcinkovich, C., Bielak, J.,., Okaya, D., Archuleta, R., Wilkins-Diehr, N., Cutchin, S., Chourasia, A., Kremenek, G., Jagatheesan, A., Brieger, L., Majundar, A., Chukkapalli, G., Xin, Q., Banister, B., Thorp, D., Kovatch, P., Diegel, L., Sherwin, T., Jordan, C., Thiebaux, M., Lopez, J. (2004) The SCEC TeraShake Earthquake Simulation Eos Trans. AGU, 85(47), Fall Meet. Suppl., Abstract SF31B-05 INVITED

Minster, J. B. and Jordan, T. H., 1978, Present-day plate motions: Journal of Geophysical Research 83, p. 5331-5354.

Mount, V. S., and Suppe, J., 1992, Present-day stress orientations adjacent to active strike-slip faults, California and Sumatra: Journal of Geophysical Research, v. 97, no. B8, p. 11,995-12,031.

Munster, J., 1997, Velocity Model of the Santa Maria Basin, CA, and its implications for seismic hazard assessment, Harvard University undergraduate thesis, 80 p.

Namson, J. and Davis, T. L. (1990). Late Cenozoic fold-and-thrust belt of the Southern Coast Ranges and Santa Maria Basin, California, AAPG Bulletin-American Association of Petroleum Geologists 74(4): 467-492.

Namson, J., and Davis, T. L., 1988a, A Structural transect of the western Transverse Ranges, California: Implications for lithospheric kinematics and seismic risk evaluation: Geology, v. 16, p. 675-679.

Olsen, K. B., 2000, Site amplification in the Los Angeles Basin from 3D modeling of ground motion, Seismological Research Letters, vol.71, no.2, pp.229-230.

Onderdonk, N. W., Minor, S. A. and Kellogg, K. S. (2005). "Taking apart the Big Pine Fault; redefining a major structural feature in Southern California." Tectonics 24(6): 11.

Pinter, N., C. C. *Sorlien, A. T.* Scott, 2003, Fault-related fold growth and isostatic subsidence, California Channel Islands, American Journal of Science, vol.303, no.4, pp.300-318.

Pitarka, A., and K. Irikura (1996). Modeling 3D surface topography by a finite-difference method: Kobe–JMA station site, Japan, case study, *Geophysical Research Letters 23*, 2729–2732.

Plesch, A., C. Tape, and J.H. Shaw, 2009, CVM-H 6.0: integration of adjoint-based tomography, the San Joaquin basin and other advances in the SCEC community velocity model, SCEC Annual Meeting, Palm Springs, CA.

Plesch, A., J. H. Shaw, C. Benson, W. A. Bryant, S. Carena, M. Cooke, J. Dolan, G. Fuis, E. Gath, L. Grant, E. Hauksson, T. Jordan, M. Kamerling, M. Legg, S. Lindvall, H. Magistrale, C. Nicholson, N. Niemi, M. Oskin, S. Perry, G. Planansky, T. Rockwell, P. Shearer, C. Sorlien, M. P. Suess, J. Suppe, J. Treiman, and R. Yeats (2007), Community Fault Model (CFM) for Southern California, *BSSA*, 97, 1793-1802.

Reed, R. D., and Hollister, J. S. (1936). Structural evolution of southern California: Tulsa, Oklahoma, American Association of Petroleum Geologists, 157 p.

Shaw, J. and J. Suppe (1994). Active faulting and growth folding in the eastern Santa Barbara Channel, California, *Geological Society of America Bulletin*, 106/5, 607-626.

Shaw, J. H., C. D. Connors, and J. Suppe (2005). *Seismic Interpretation of Contractional Fault-related folds*: AAPG Seismic Atlas, Studies in Geology #53, Tulsa, Oklahoma, American Association of Petroleum Geologists, 156 p.

Shearer, P., E. Hauksson, and G. Lin (2005). Southern California hypocenter relocation with waveform cross correlation: Part 2. Results using source-specific station terms and cluster analysis, *Bull. Seismol. Soc. Am*., **95**, 904-915, doi: 10.1785/0120040168, 2005.

Süss, P., and J. H. Shaw, P wave seismic velocity structure derived from sonic logs and industry reflection data in the Los Angeles basin, California, *Journal of Geophysical Research 108*(B3), doi:10.1029/2001JB001628.

Suppe, J., and D. A. Medwedeff (1990). Geometry and kinematics of fault propagation folding, *Ecologae Geol. Helv.* **83,** no. 3, 409–454.

Tape, C., Q. Liu, A. Maggi, and J. Tromp (2009), Adjoint tomography of the southern California crust, Science, 325, 988–992.

Tape, C., Q. Liu, A. Maggi, and J. Tromp (2010), Seismic tomography of the southern California crust based on spectral-element and adjoint methods, Geophys. J. Int., 180, 433–462.

Tromp, J., C. Tape, and Q. Liu (2005), Seismic tomography, adjoint methods, time reversal, and bananadoughnut kernels, Geophys. J. Int., 160, 195–216.

Vedder, J. G.; Wagner, H. C. and Schoellhamer, J. E., 1969, Geological framework of the Santa Barbara Channel region, *in* Geology, Petroleum Development and Seismicity of the Santa Barbara Channel Region, California: U. S. Geological Society Professional Paper 679-A, p.1-11.

Wackernagel, H., Multivariate Statistics, 1998, An introduction with Applications, 257 pp., Springer-Verlag, New York.

Ward, S. N., 2007, "Methods for evaluating earthquake potential and likelihood in and around California." Seismological Research Letters 78(1): 121-133.

WGCEP, 2007, Working Group on California Earthquake Probabilities Final Report, CEA, USGS, SCEC.

Yeats, R. S., 1983, Large-scale Quaternary detachments in Ventura basin, southern California: Journal of Geophysical Research, v. 88, no. B1, p. 569-583.

Yeats, R. S., 1988, Late Quaternary slip rate on the Oak Ridge fault, Transverse Ranges, California, Implications for seismic risk: Journal of Geophysical Research, v. 93, p. 12,137-12,159.

Yeats, R. S., Huftile, G. J., 1995, The Oak Ridge fault system and the 1994 Northridge earthquake, Nature, 373, 418-420.

Yeats, R. S., Huftile, G. J., and Grigsby, F. B., 1988, Oak Ridge fault, Ventura fold belt, and the Sisar decollement, Ventura basin, California: Geology, v. 16, p. 1113-1116.

Zoback, M. D., Zoback, M. L., Mount, V. S., Suppe, J., Eaton, J. P., Healy, J. H., Oppenheimer, D., Rosenberg, P., Jones, L., Raleigh, C. B., Wong, I. G., Scotti, O., and Wentworth, C., 1987, New Evidence on the state of stress of the San Andreas fault system: Science, v. 238, p. 1115-111.

Bibliography of publications resulting from this work

Nicholson, C., Plesch, A., Shaw, J.H. and E. Hauksson (2012), Upgrades and Improvements to the SCEC Community Fault Model: Increasing 3D fault complexity and compliance with surface and subsurface data, SCEC Annual Meeting XII Program, p.125-126.

Plesch, A., J. Munster, and J.H., Shaw, A structural velocity model of the Santa Maria basin, California, Bulletin of the Seismological Society of America, (in prep).